NREL
NATIONAL RENEWABLE ENERGY LABORATORY

Validation of GOES-Derived Surface Radiation Using NOAA's Physical Retrieval Method

A. Habte, M. Sengupta, and S. Wilcox
National Renewable Energy Laboratory

NREL is a national laboratory of the U.S. Department of Energy, Office of Energy Efficiency & Renewable Energy, operated by the Alliance for Sustainable Energy, LLC.

Technical Report
NREL/TP-5500-57442
January 2013

Contract No. DE-AC36-08GO28308

NREL
NATIONAL RENEWABLE ENERGY LABORATORY

Validation of GOES-Derived Surface Radiation Using NOAA's Physical Retrieval Method

A. Habte, M. Sengupta, and S. Wilcox
National Renewable Energy Laboratory

Prepared under Task No. SS10.1620

National Renewable Energy Laboratory
15013 Denver West Parkway
Golden, Colorado 80401
303-275-3000 • www.nrel.gov

Technical Report
NREL/TP-5500-57442
January 2013

Contract No. DE-AC36-08GO28308

NOTICE

Available electronically at http://www.osti.gov/bridge

Available for a processing fee to U.S. Department of Energy
and its contractors, in paper, from:

U.S. Department of Energy
Office of Scientific and Technical Information
P.O. Box 62
Oak Ridge, TN 37831-0062
phone: 865.576.8401
fax: 865.576.5728
email: mailto:reports@adonis.osti.gov

Available for sale to the public, in paper, from:

U.S. Department of Commerce
National Technical Information Service
5285 Port Royal Road
Springfield, VA 22161
phone: 800.553.6847
fax: 703.605.6900
email: orders@ntis.fedworld.gov
online ordering: http://www.ntis.gov/help/ordermethods.aspx

Cover Photos: (left to right) PIX 16416, PIX 17423, PIX 16560, PIX 17613, PIX 17436, PIX 17721

Printed on paper containing at least 50% wastepaper, including 10% post consumer waste.

Foreword

This report was part of a multiyear collaboration with the University of Wisconsin and the National Oceanic and Atmospheric Administration (NOAA) to produce high-quality, satellite-based, solar resource datasets for the United States under National Renewable Energy Laboratory (NREL) subcontract no. AXL-0-40276-01. NOAA had initially developed the Global Solar Insolation Project to estimate solar global horizontal irradiance (GHI) from satellites primarily for coral bleaching and other applications that did not require subhourly data at a high resolution. Direct normal irradiance (DNI) was not an output of the model. The subcontract resulted in the creation of cloud property and solar radiation datasets (including both GHI and DNI) at half-hourly intervals with a nominal resolution of 4 km. This report evaluates this newly developed, satellite-based, solar radiation dataset using surface measurements of solar radiation as input.

Preface

High-quality, solar resource assessment accelerates technology deployment by making a positive impact on decision making and reducing uncertainty in investment decisions. Satellite-based solar resource datasets are used as a primary source in solar resource assessment. This is mainly because satellites provide larger areal coverage and longer periods of record than ground-based measurements. With the advent of newer satellites with increased information content and faster computers that can process increasingly higher data volumes, methods that were considered too computationally intensive are now feasible. One class of sophisticated methods for retrieving solar resource information from satellites is a two-step, physics-based method that computes cloud properties and uses the information in a radiative transfer model to compute solar radiation. This method has the advantage of adding additional information as satellites with newer channels come on board. This report evaluates the two-step method developed at NOAA and adapted for solar resource assessment for renewable energy with the goal of identifying areas that can be improved in the future.

Acknowledgments

We would like to thank Thomas Stoffel, Solar Resources and Forecasting Group manager, for his leadership, support, and guidance; Daryl Myers (NREL, retired) for his continuous, insightful suggestions and support; and Mike Dooraghi for reviewing this report.

List of Acronyms

AOD	aerosol optical depth
CSP	concentrating solar power
DNI	direct normal irradiance
GFS	Global Forecast System
GHI	global horizontal irradiance
GOES	Geostationary Operational Environmental Satellite
GSIP	Global Solar Insolation Project
ISIS	Integrated Surface Insolation Study
MBE	mean bias error
NOAA	National Oceanic and Atmospheric Administration
NREL	National Renewable Energy Laboratory
PV	photovoltaic
RMSE	root mean square error
SASRAB	Satellite Algorithm for Shortwave Radiation Budget
SOLRMAP	Proprietary Solar Resource and Meteorological Assessment Project
SURFRAD	Surface Radiation

Executive Summary

A comparison of satellite-derived solar resource with nine high-quality, ground-based solar radiation measurements from NOAA's Surface Radiation (SURFRAD) Network, the Integrated Surface Insolation Study (ISIS) Network, the Solar Radiation Research Laboratory (SRRL) at NREL, and DOE's Solar Resource and Meteorological Assessment Project (SOLRMAP) program was conducted. The comparison was made using data from 2009 for various locations. Our results showed that the satellite-based method underpredicted both global horizontal irradiance (GHI) and direct normal irradiance (DNI). GHI values were underestimated by about 13% to 22% for the stations located in a desert environment, such as Desert Rock, Nevada, and SOLRMAP stations located around southwest Nevada and Arizona. We found that the Satellite Algorithm for Shortwave Radiation Budget (SASRAB) radiative transfer model caused the underprediction of GHI and DNI, especially in clear-sky situations and low zenith angles (around solar noon). Using other radiative transfer algorithms reduced the bias from SASRAB, and it is expected that the accuracy of the satellite-based product will significantly improve with the introduction of a high-quality, radiative transfer model. Future work will aim to reduce the biases by using better input parameters and applying these parameters to a better, simple, clear-sky radiative transfer model that properly accounts for the parameters.

Table of Contents

List of Figures

List of Tables

1 Introduction

Understanding system performance, reducing integration cost, and achieving higher penetration of concentrating solar power (CSP) and photovoltaic (PV) projects requires accurate knowledge of the available solar resource. Critical to this knowledge is an understanding of the characteristics of the incoming DNI and GHI. Knowledge of the impacts of clouds, angle of incidence, spectral distribution, and intra-hour and seasonal variability is essential to accurately design utility-scale CSP and PV systems. Ground-measured solar data and/or satellite-derived solar data are essential components to understand incoming solar resources. For the last few decades, solar models have been in development to quantify the solar resource reaching the earth's surface. These models are classified as empirical or physical. This study analyzes the performance and accuracy of the output from the physics-based Global Solar Insolation Project (GSIP) model that has been used to characterize the solar radiation resource across the United States. GSIP datasets for the United States are created using measurements from the Geostationary Operational Environmental (GOES) series of satellites. The GSIP model computes solar irradiance at 4x4-km resolution using the visible and infrared channels of GOES [1]. The temporal and spatial evaluation was performed by comparing the GSIP modeled data to concurrent ground-based measurements. Surface measurements were obtained from NOAA's SURFRAD (www.srrb.noaa.gov/surfrad/sitepage.html) and ISIS (www.srrb.noaa.gov/isis/isissites.html), SRRL at NREL (www.nrel.gov/midc/srrl_bms/), Sun Spot One (SS1) (www.nrel.gov/midc/ss1/), and proprietary SOLRMAP stations. We considered only high-quality, ground-based solar data because the quality of data is important in evaluating solar models [12]. The term "high-quality" is used to indicate that station radiometers undergo periodic, quality, routine maintenance and calibrations traceable to the world radiometric reference (with typical uncertainty 2% to 5% for such radiometers, Table 1) [2] [3] [4] [5] [6].

The GSIP model uses geostationary, satellite-derived measurements in the visible and infrared parts of the spectrum in conjunction with atmospheric profiles from the Global Forecast System (GFS) weather prediction model to retrieve cloud optical characteristics [17]. This information is an input to a fast radiative transfer model to calculate radiative fluxes. Unlike empirical models based on correlations between surface radiation and satellite measurements, the GSIP model is physics based and explicitly accounts for nonlinear interactions between clouds and solar radiation [1] [15] [16]. The scarcity of ground-based measurement stations and reported inaccuracies in empirical model results makes the GSIP model a viable alternative to provide accurate spatial and temporal irradiance information on a larger scale. The model was run for multiple years for surface radiation, and this study is a preliminary validation of GHI retrieved using the GSIP model for 2009.

2 Method and Result

Ground-measured and derived data are complementary to each other. Ground-measured data is inadequate because there are a very limited number of measurement stations in long-term operation (especially high-quality stations). To fill the gap, modeled data, such as GSIP, provides global coverage of solar data. However, quality, ground-based solar data provides an excellent tool to verify the temporal and spatial accuracy of the satellite-based algorithm. We therefore selected sites located at NREL (SRRL); SS1; Desert Rock, Nevada; and Hanford, California; and

five SOLRMAP proprietary stations located in southern Colorado, southwest Arizona, and Nevada.

Ground-measured and GSIP-estimated GHI data were compared for these nine locations. A broad filtering was carried out before the comparison analysis to remove outliers and high-zenith-angle datasets (greater than 75 degrees). Results of differences were calculated as modeled minus ground-based measurements (negative values indicated the model was low). These stations were chosen because the ground-based data was of high quality, so deemed because the instruments are well calibrated and maintained. The stations are equipped with silicon or thermopile instruments, and the uncertainty of the data from these sensors ranges from 2% to 5% (Table 1).

Table 1. Station Location and Description

Station	Latitude	Longitude	Description	Instrument Type	Uncertainty Estimates*
NREL, Golden, CO	39.74	-105.18	NREL	Thermopile	2%–5%
Hanford, CA	36.31	-119.63	NOAA/ISIS	Thermopile	2%–5%
Desert Rock, NV	36.63	-116.02	NOAA/SURFRAD	Thermopile	2%–5%
SS1, Monte Vista, CO	37.56	-106.09	San Luis Valley Developers Group, the Governor's Energy Office, and NREL	Rotating Shadowband Radiometers	5%
A	**Proprietary Stations**		Southern Colorado	Rotating Shadowband Radiometers	5%
B			Southwest Arizona	Rotating Shadowband Radiometers	5%
C			Southwest Arizona	Rotating Shadowband Radiometers	5%
D			Southwest Arizona	Rotating Shadowband Radiometers	5%
E			Southwest Nevada	Rotating Shadowband Radiometers	5%

The surface data was averaged from 5 minutes to 120 minutes at 5-minute intervals to represent the spatial extent of the satellite pixel. The 4x4-km GSIP data is available every 30 minutes. The averages and statistical outputs were used to compare the two datasets. From the perspective of the down-looking satellite, ground-based measurements represent a relatively small area above the measurement station and are commonly available at a time resolution of 1 minute, which is significantly faster than that available from satellite models. The high-frequency, ground-based

measurements are very useful for numerous solar resource applications [13], such as irradiance variability during short time intervals.

The GSIP data had about 60 output parameters; however, only the GHI, DNI, and cloud type were used in this evaluation (Figure 1). For the analysis, the cloud type data from the satellite was used for the clear- and cloudy-sky classification.

A

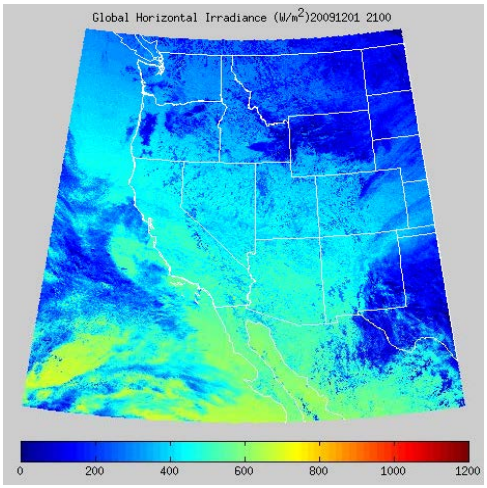

B

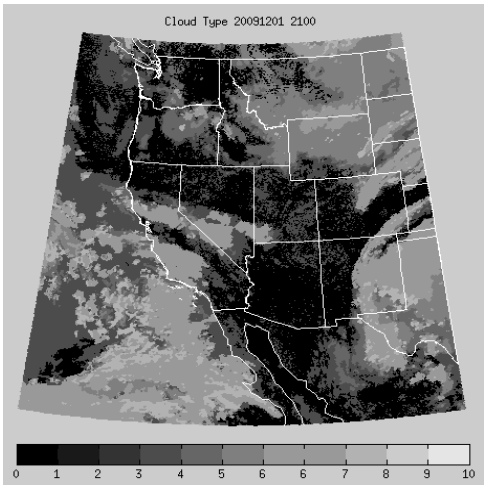

Figure 1. GSIP modeled output for (A) GHI and (B) cloud type for the Western United States for December 1, 2009, at 2100 UTC. Cloud type specifications: Clear (0), PROB_clear (1), FOG (2), WATER (3), SUPERCOOLED (4), MIXED (5), OPAQUE_ICE (6), THINICE (6), CIRRUS (7), OVERLAP (8), OVERSHOOTING (9), UNKNOWN (10).

Figure 2, Figure 3, Table 2, and the appendix demonstrate the differences between the GSIP modeled and ground-measured data. Clear and cloudy conditions were compared separately, with ground-measured data averaged from 5 minutes to 2 hours at 5-minute intervals centered on the satellite measurement time (30 minutes). The satellite spatial resolution was 4x4 km. Therefore, it should be noted that subpixel variability in clouds and surface radiation cannot be captured using the satellite datasets (e.g., the varying effects from passing popcorn cumulus clouds).

The frequency distribution of the differences between the ground-based measurements and the GSIP GHI data is important in determining the performance of the GSIP modeled data. The distribution, represented by "W/m^2," appeared to fall on average between -150 W/m^2 to 50 W/m^2 for most stations. (Refer to the appendix.) This difference shows that the modeled data underestimated irradiance data relative to the high-quality, ground-based data.

A

A

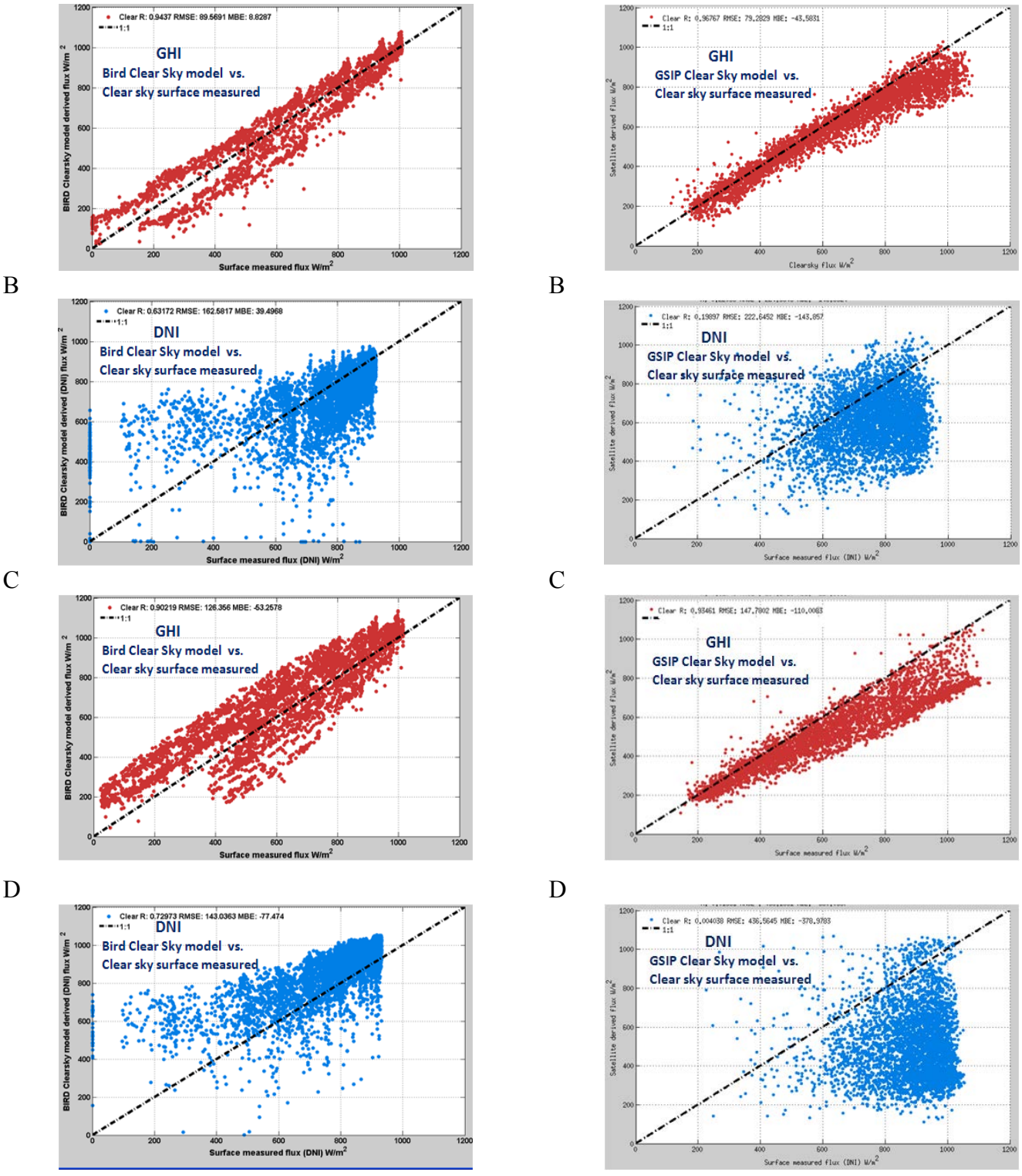

Figure 2. Scatter plots showing the difference between the BIRD model and GSIP model compared to the ground-based measurements under clear-sky conditions: Hanford, California (A (GHI) and B (DNI)), Desert Rock, Nevada (C (GHI) and D (DNI). The units of RMSE and MBE described on the legend are in W/m^2.

For cloudy conditions, as might be expected, the differences showed a higher scatter and a lower correlation coefficient between measured and satellite-estimated irradiance data. (Refer to the appendix.) For instance, the correlation was 0.91, 0.86, 0.83, and 0.80 for Hanford, California; Desert Rock, Nevada; NREL; and SS1stations under cloudy conditions, versus 0.97, 0.93, 0.96, and 0.96 under clear conditions, respectively (Table 2).

Unlike other stations, the desert stations—such as Desert Rock, Nevada; southwest Arizona;\, and other Nevada sites that are clearer sites—appeared to have lower correlation. The reason for this is not clear. The GSIP model reported lower GHI for clear-sky events, especially around solar noon, when the irradiance values were the highest.

The relative root mean square error (RMSE) and mean bias error (MBE) percentages are a statistical measure of random-like differences between the ground-measured data and the GSIP satellite data. The nine locations had lower RMSE percentages, and Desert Rock, Nevada, and Hanford, California, had higher MBE percentages, for the clear-sky condition than the cloudy periods. The higher bias, where the model underestimated irradiance during clear-sky events, could be related to model misspecification or miscalculation of aerosol optical depth (AOD) and ground albedo. Overall, the results of the bias from this study were similar to the study done by [9], which compared empirical models to ground-based measurements.

As shown in Figure 2 and scatter plots described in the appendix, the GSIP model data appeared to lie below the 1:1 line, particularly under clear-sky conditions, which indicates that the ground-based measurements were often higher than the GSIP modeled data. To understand this situation, the GSIP model was also compared to the BIRD clear-sky model [10] under clear-sky conditions. The results show that the GSIP model underperformed under clear-sky conditions for GHI and DNI. Figure 2 and Table 2 (yellow) also show the percentage bias for GHI under clear-sky conditions. This underestimation of irradiance by the model was more noticeable for the desert environment stations (Table 2, blue). The DNI bias was also more apparent for the Desert Rock, Nevada, station (Figure 2). Therefore, the model requires refinement in addressing these situations, and areas for further investigation could include greater accuracy in clear-sky, ground albedo, aerosol estimates, water vapor estimates, and clear-sky optical properties.

In this study, we also investigated the time averages of the ground-measured data that best related to the satellite time interval. A satellite pixel represents a nominal 4-km-square area; whereas a ground-based measurement represents only a point on the ground. Therefore, we took various time averages of the ground-based measurements to examine which time average periods best matched the time interval centered on the GSIP measurement time. Figures in the appendix show that the systematic (bias) differences were relatively constant for all averaging periods. In most cases, the random differences or RMSE decreased as the averaging period increased, probably because of the cancellation of some of the random differences during longer periods of time. The 60-minute time average appeared to be a reasonable averaging period to compare the ground-based GHI measurement data to the GSIP GHI data. However, it should be noted that for cloudy conditions at Desert Rock, Nevada, and Station B, the correlation between ground-based and satellite measurements improved beyond the 60-minute average time period.

Table 2. Annual Statistics (2009) of Correlation (R), Relative MBE (%), and RMSE (%) for Comparing Ground-Based Measurements Averaged to 30 Minutes, 60 Minutes, and 120 Minutes and Satellite-Derived (30 minutes) GHI Data.

Cloud Type	Annual Statistics	Hanford, CA			Desert Rock, NV			NREL, CO			SS1, CO		
		30-min average	60-min average	120-min average	30-min average	60-min average	120-min average	30-min average	60-min average	120-min average	30-min average	60-min average	120-min average
	R	0.89	0.9	0.9	0.84	0.84	0.86	0.86	0.87	0.86	0.83	0.84	0.85
	MBE	-7.48	-7.64	-9.51	-17.66	-17.74	-18.85	-11	-12.2	-16.16	-13.07	-14.43	-18.18
All	RMSE	20.39	20.22	21.67	27.02	26.39	26.96	28.04	28.07	31.05	28.16	28.39	31.31
	R	0.9	0.91	0.92	0.84	0.86	0.88	0.82	0.83	0.82	0.78	0.8	0.79
	MBE	0.85	0.85	0.59	-6.35	-5.91	-5.71	-9.53	-9.39	-9.4	-11.87	-11.91	-12.33
Cloudy	RMSE	20.23	19.13	19.07	24.64	22.7	22.13	29.26	28.05	27.95	29.87	28.87	29.33
	R	0.97	0.97	0.96	0.93	0.93	0.94	0.96	0.96	0.96	0.95	0.96	0.95
	MBE	-7.01	-7	-7.41	-17.53	-17.17	-16.87	-8.11	-8.2	-8.52	-8.67	-8.82	-8.99
Clear	RMSE	11.89	11.89	12.58	21.8	21.52	21.14	12.51	12.42	13.18	13.37	13.12	13.29

Cloud Type	Annual Statistics	A			B			C			D			E		
		30-min average	60-min average	120-min average	30-min average	60-min average	120-min average	30-min average	60-min average	120-min average	30-min average	60-min average	120-min average	30-min average	60-min average	120-min average
	R	0.82	0.84	0.85	0.85	0.86	0.87	0.84	0.86	0.87	0.85	0.87	0.87	0.79	0.81	0.82
	MBE	-18.02	-17.34	-20.83	-20.45	-21.6	-24.75	-19.58	-20.8	-23.96	-12.62	-13.88	-17.29	-14.96	-16.41	-20.17
All	RMSE	30.44	29.24	31.99	28.24	28.61	30.79	28.1	28.56	30.78	23.93	24.4	27	28.27	28.81	31.29
	R	0.79	0.81	0.79	0.85	0.87	0.88	0.86	0.87	0.87	0.87	0.89	0.89	0.74	0.75	0.75
	MBE	-23.96	-14	-14.59	-7.49	-7.62	-8.4	-6.86	-7.03	-7.69	-2.55	-2.83	-3.73	-15.44	-15.6	-16.23
Cloudy	RMSE	30.4	28.67	29.23	23.94	22.52	21.87	23.68	22.4	22	22.28	20.71	20.75	31.42	31.2	30.91
	R	0.94	0.95	0.94	0.95	0.95	0.95	0.93	0.94	0.93	0.92	0.92	0.92	0.89	0.89	0.87
	MBE	-12.91	-12.9	-12.93	-22.39	-22.52	-22.83	-21.49	-21.59	-21.91	-13.02	-13.16	-13.5	-13.44	-13.51	-13.86
Clear	RMSE	16.3	16.28	16.32	24.29	24.18	24.29	24.04	23.93	24.08	18.46	18.37	18.59	21.91	21.62	21.79

The differences (MBE%, RMSE%, and R) on a monthly average basis were also analyzed (Figure 3), and the results were consistent, as mentioned above. In most cases, the MBE% was lower during summer months than the rest of the year. Zenith angle effects in both modeled and measured data in the winter months may have contributed to higher MBE in those months. In most stations, RMSE was lower for the majority of months under clear conditions than cloudy conditions. Further, the magnitude of RMSE difference between clear and cloudy conditions for each month was smaller for the desert environment, such as the Desert Rock, Nevada, station, than the relatively cloudier stations, such as NREL and SS1; however, differences in the MBE had the opposite effect.

A

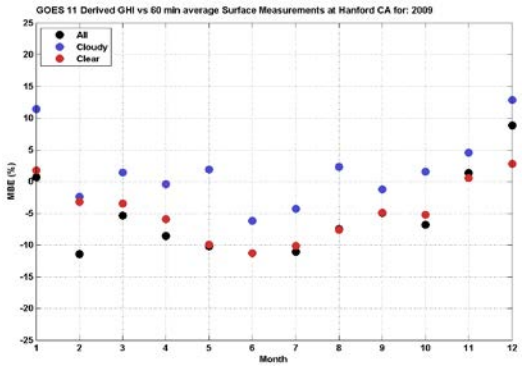
GOES 11 Derived GHI vs 60 min average Surface Measurements at Hanford CA for: 2009
All
Cloudy
Clear
MBE (%)
Month

A

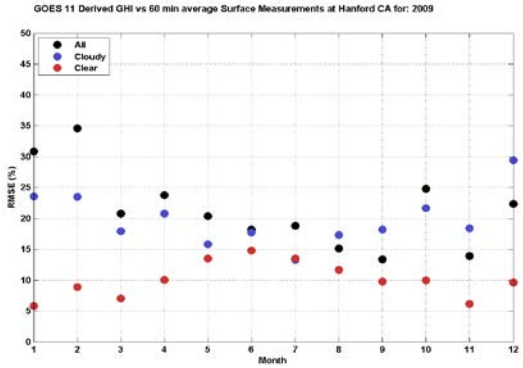
GOES 11 Derived GHI vs 60 min average Surface Measurements at Hanford CA for: 2009
All
Cloudy
Clear
RMSE (%)
Month

B

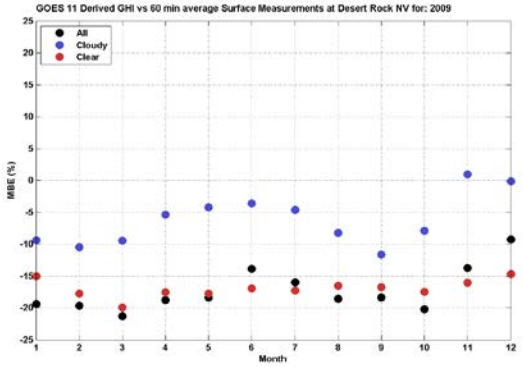
GOES 11 Derived GHI vs 60 min average Surface Measurements at Desert Rock NV for: 2009
All
Cloudy
Clear
MBE (%)
Month

B

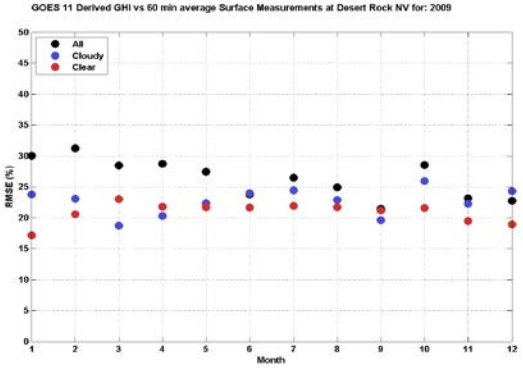
GOES 11 Derived GHI vs 60 min average Surface Measurements at Desert Rock NV for: 2009
All
Cloudy
Clear
RMSE (%)
Month

C

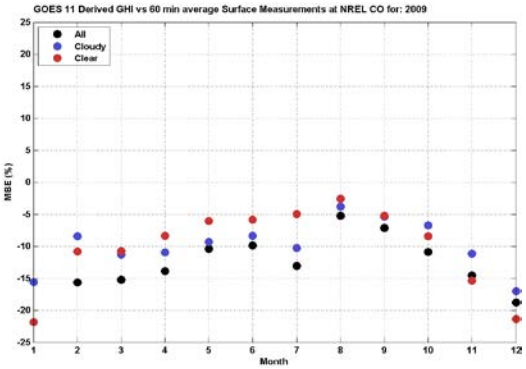
GOES 11 Derived GHI vs 60 min average Surface Measurements at NREL CO for: 2009
All
Cloudy
Clear
MBE (%)
Month

C

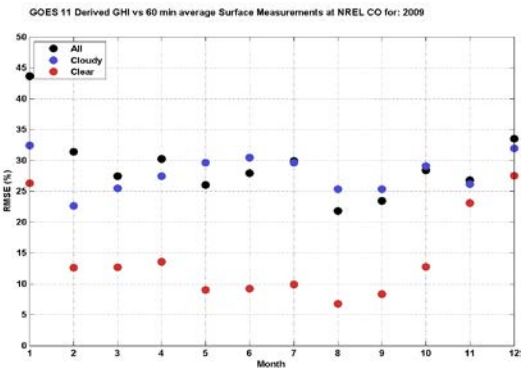
GOES 11 Derived GHI vs 60 min average Surface Measurements at NREL CO for: 2009
All
Cloudy
Clear
RMSE (%)
Month

D

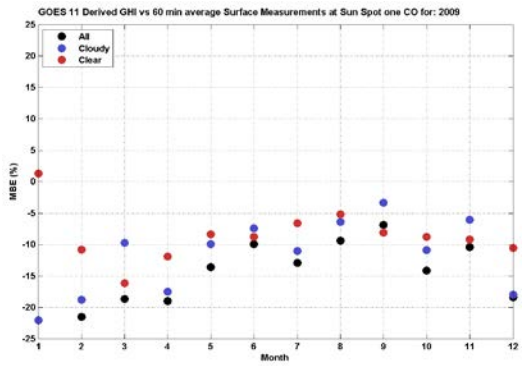
GOES 11 Derived GHI vs 60 min average Surface Measurements at Sun Spot one CO for: 2009
All
Cloudy
Clear
MBE (%)
Month

D

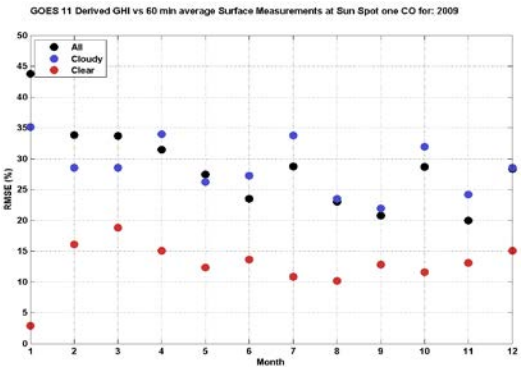
GOES 11 Derived GHI vs 60 min average Surface Measurements at Sun Spot one CO for: 2009
All
Cloudy
Clear
RMSE (%)
Month

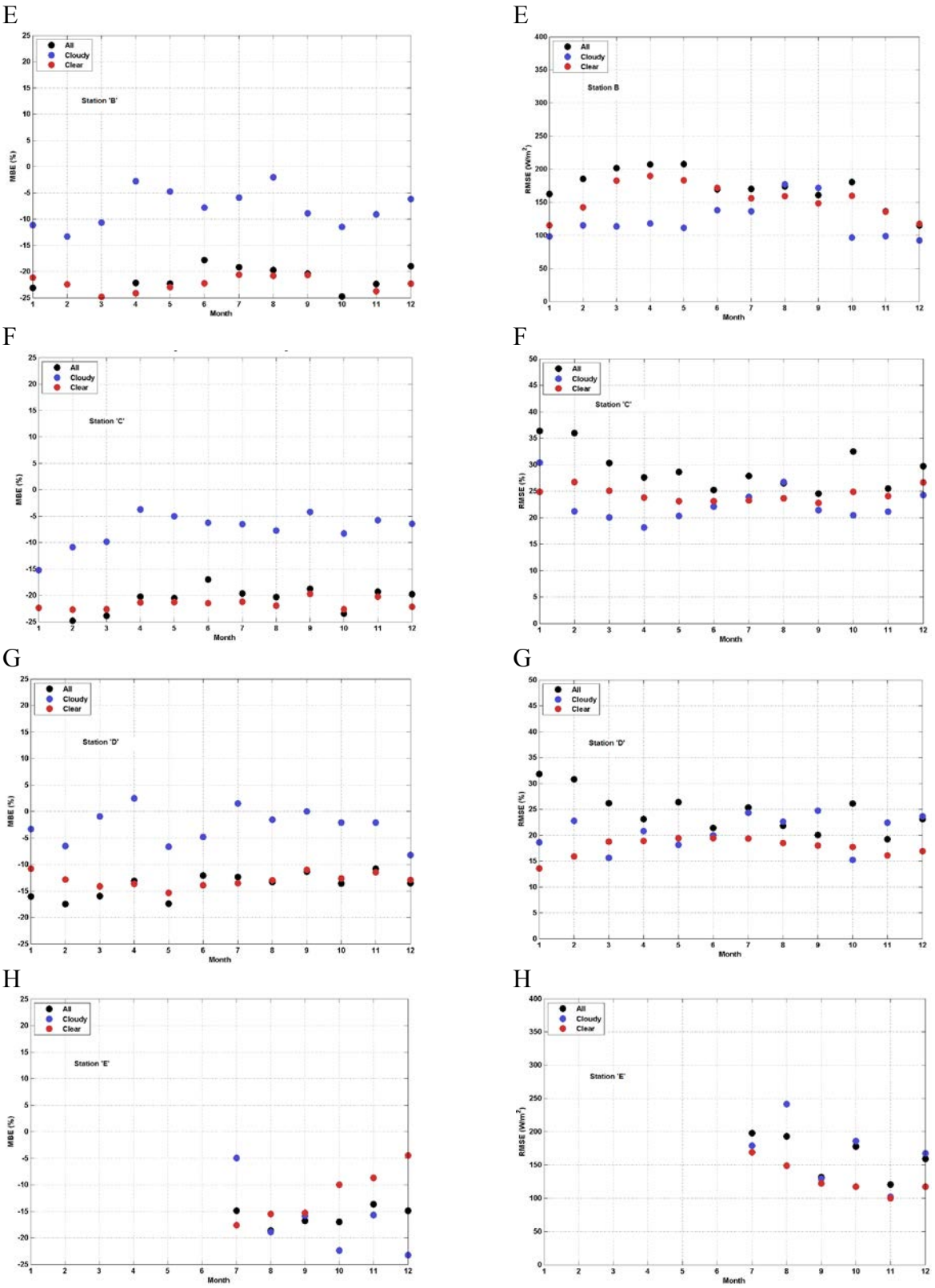

Figure 3. GHI monthly MBE% and RMSE% for (A) Hanford, California; (B) Desert Rock, Nevada; (C) NREL; (D) SS1; (E) B; (F) C; (G) D; and (H) E stations.

3 Summary

The qualities of the GSIP satellite-derived data make it possible to deliver location-specific and reliable time-series solar resource data. The GSIP physical model had a higher spatial (4-km) and temporal (30-minute) resolution dataset than some other empirical-based model data, such as the hourly and 10-km resolution State University of New York Perez model [11] and the European METEOSAT–based Heliostat model [12]. Greater spatial resolution will be beneficial to more accurate solar resource data for CSP and PV projects in areas of high spatial variability [12], [13]. The GSIP averages of clear GHI data demonstrated better correlation to ground-based, clear-sky data than averages from the cloudy periods, but clear-sky averages had a greater bias, generally negative. Moreover, the ground-measured data performed better than the GSIP model in capturing the short-term variability of irradiance for a narrow integrated time interval for a specific point on the earth's surface. However, satellite-based surface radiation datasets are primarily useful for long-term solar resource assessment applications, and in that area the model should be competent once bias issues are addressed. The model requires refinement in addressing clear-sky, ground albedo, aerosol estimates, water vapor estimates, and clear-sky optical properties. Aerosols are external datasets that can be provided to the model, and more recent aerosol databases may be used to improve performance. The surface albedo became an issue in the current GSIP radiative transfer model [14]. This surface albedo was calculated from the visible satellite channel when a clear-sky point was detected. Elevated albedos showed up under certain sun satellite geometries, and those situations resulted in lower GHI than actual in the current radiative transfer scheme.

This study is an important step in decreasing the GSIP satellite data uncertainty, mainly driven by systematic deviation. Therefore, future investigation of the GSIP model will be performed by comparing the model to other empirical models and more extensive comparisons with high-quality, ground-based measurements. Further, incorporating a larger number of parameters from the GSIP modeled output in such evaluations could help identify sources of discrepancies between the model's performance and ground-based measurements. Work continues to produce estimated DNI and diffuse from the model, and a future report will evaluate performance for those parameters. Future work will also include addressing the use of better aerosol data and albedo estimates and applying them to a better clear-sky radiative transfer model that properly accounts for the parameters.

References

[1] Sengupta, M.; Heidinger, A.; Miller, S. "Validating an Operational Physical Method to Compute Surface Radiation From Geostationary Satellites." *Proceedings of SPIE—The International Society for Optical Engineering, Volume 7773*; Aug. 3–5, 2010, San Diego, California. Bellingham, WA: SPIE. NREL/CP-550-48808. Golden, CO: National Renewable Energy Laboratory, 2010.

[2] Reda, I. *Method to Calculate Uncertainty Estimate of Measuring Shortwave Solar Irradiance using Thermopile and Semiconductor Solar Radiometers.* NREL/TP-3B10-52194. Golden, CO: National Renewable Energy Laboratory, 2011.

[3] Stoffel, T. L.; Myers, D. R. "Accuracy of Silicon Versus Thermopile Radiometers for Daily and Monthly Integrated Total Hemispherical Solar Radiation." Paper No. 777314. Dhere, N.G.; Wohlgemuth, J.H.; Lynn, K.; eds. "Reliability of Photovoltaic Cells, Modules, Components, and Systems III." *Proceedings of SPIE—The International Society for Optical Engineering, Volume 7773*; August 3–5, 2010, San Diego, California. Bellingham, WA: SPIE. NREL/CP-550-48697. Golden, CO: National Renewable Energy Laboratory, 2010.

[4] Wilcox, S. M.; Myers, D.R. *Evaluation of Radiometers in Full-Time Use at the National Renewable Energy Laboratory Solar Radiation Research Laboratory.* NREL/TP-550-44627. Golden, CO: National Renewable Energy Laboratory, 2008.

[5] Myers, D.R.; Reda, I.M.; Wilcox, S.M.; Stoffel, T.L. "Uncertainty Analysis for Broadband Solar Radiometric Instrumentation Calibrations and Measurements: An Update," Preprint. Prepared for the World Renewable Energy Congress VIII, Aug. 29–Sept. 3, 2004. CP-560-36201. Golden, CO: National Renewable Energy Laboratory, 2004.

[6] King, D.L.; Myers, D.R. "Silicon-Photodiode Pyranometers: Operational Characteristics, Historical Experiences, and New Calibration Procedures." *Conference Record of the Twenty Sixth IEEE Photovoltaic Specialists Conference*, Sept. 29–Oct. 3, 1997, Anaheim, California, pp. 1,285–1,288. NREL/CP-24945. Golden, CO: National Renewable Energy Laboratory, 1997.

[7] Wilcox, S.; Myers, D. "Joint Solar Power Industry and Department of Energy Solar Resource and Meteorological Assessment Project [SOLRMAP]." Tsai, B.K. *Optical Modeling and Measurements for Solar Energy Systems III, Proceedings of SPIE— The International Society for Optical Engineering, Volume 7410*; San Diego, California. Bellingham, WA: SPIE. NREL/CP-550-46537. Golden, CO: National Renewable Energy Laboratory, 2009.

[8] Vignola. "Variability of Solar Radiation Data Over Short Time Intervals." *Proceedings of Solar 2001, American Solar Energy Society Conference*; 2001, Washington, DC.

[9] Myers, D.R.; Wilcox, S.; Marion, W.; George, R.; Anderberg, M. "Broadband Model Performance for an Updated National Solar Radiation Database in the United States of America." *Proceedings of Solar World Congress, International Energy Society*; 2005.

[10] Bird, R.E.; Hulstrom, R.L. *Simplified Clear Sky Model for Direct and Diffuse Insolation on Horizontal Surfaces.* SERI/TR-642-761. Golden, CO: Solar Energy Research Institute, 1981.

[11] Perez, R.; Ineichen, P.; Moore, K; Kmiecik, M.; Chain, C.; George, R.; Vignola, F. "A New Operational Satellite-to-Irradiance Model—Description and Validation." *Solar Energy* (73:5), 2002; pp. 307–317.

[12] Rigollier, C.; Lefèvre M.; Wald, L. "The Method Heliostat-2 for Deriving Shortwave Solar Radiation From Satellite Images." *Solar Energy* (77:12), 2004; 159–169.

[13] Gueymard, C.; Wilcox, S. "Assessment of Spatial and Temporal Variability in the U.S. Solar Resource From Radiometric Measurements and Predictions From Models Using Ground-Based or Satellite Data." *Solar Energy* (85), 2011; pp. 1,068–1,084.

[14] Pinker, R.T.; Laszlo, I. "Modeling of Surface Solar Irradiance for Satellite Applications on a Global Scale." *Journal of Applied Meteorology and Climatology* (31), 1992; pp. 194–211.

[15] Pinker, R.T.; Laszlo, I.; Tarpley, J.D.; Mitchell, K. "Geostationary Satellite Parameters for Surface Energy Balance." *Advances in Space Research* (30), 2002; 2,427–2,432.

[16] Lazlo, I.; Ciren, P.; Liu, H.; Kondragunta , S.; Tarpley, J.D.; Goldberg, M.D. "Remote Sensing of Aerosol and Radiation From Geostationary Satellites." *Advances in Space Research* (41), 2008; 1,882–1,893.

[17] Miller, S.D.; Rogers, M.A.; Heidinger, A.; Laszlo, I.; Sengupta, M. "Cloud Advection Schemes for Short-Term Satellite-Based Insolation Forecasts." *Proceedings of the World Renewable Energy Forum*; 2012, Denver, Colorado (CD-ROM). Boulder, CO: American Solar Energy Society.

Appendix: Comparison Result Plots

The following plots demonstrate the relative differences between the ground-measured data and the GSIP satellite–derived data. The plots are scatter, probability distribution, and time-averaged, with one page per station. The plots are essential in understanding the differences between the two datasets; however, readers should take into consideration the stated uncertainty of the ground-measured data (Table 1), which is approximately in the 2% to 5% range. The interpretation of the uncertainty values is that the difference between the two datasets could move up and down by the uncertainty magnitude and not be significant.

A

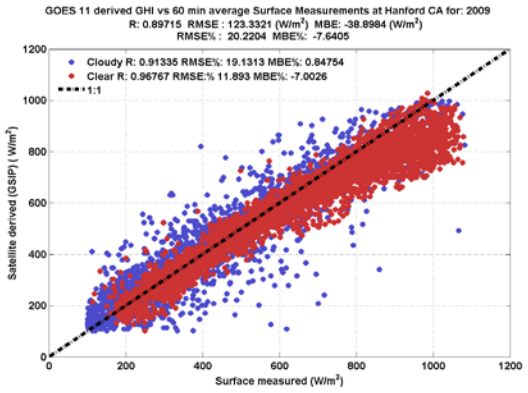

B

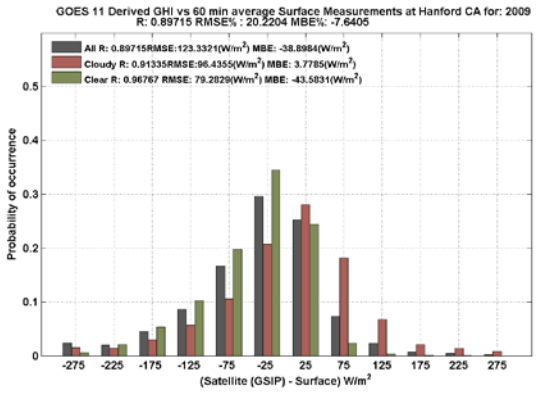

Figure A1. (A) Scatter plot and (B) probability distribution under clear and cloudy conditions for the Hanford, California, site.

C

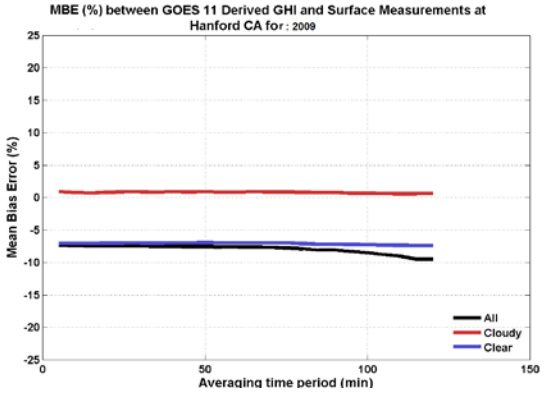

D

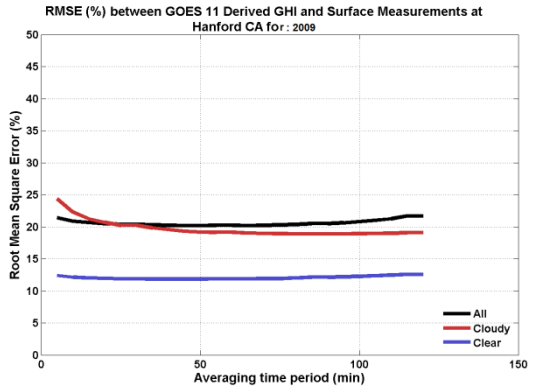

E

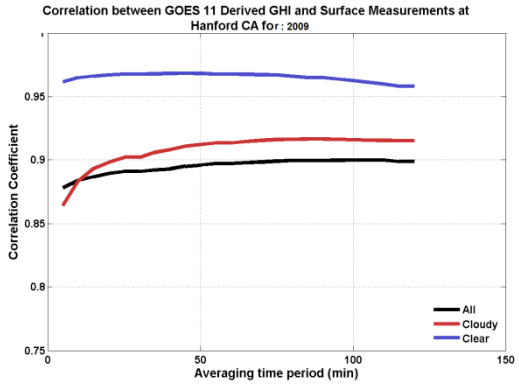

Figure A2. (C) MBE%, (D) RMSE%, and (E) correlation values under cloudy, clear, and all conditions for the Hanford, California, site.

A

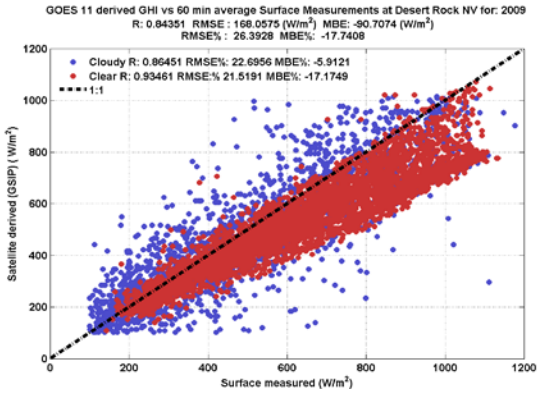

B

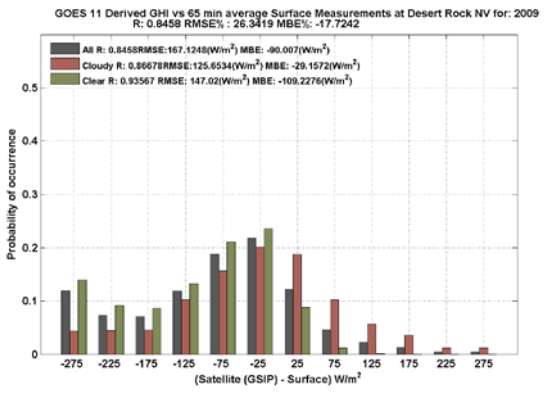

Figure A3. (A) Scatter plot and (B) probability distribution under clear and cloudy conditions for the Desert Rock, Nevada, site.

C

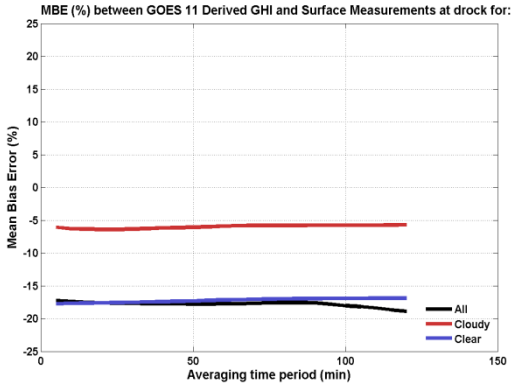

D

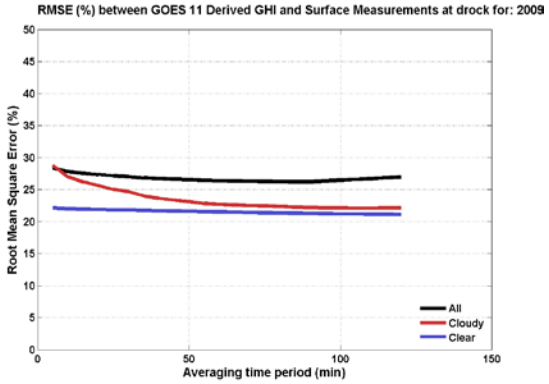

E

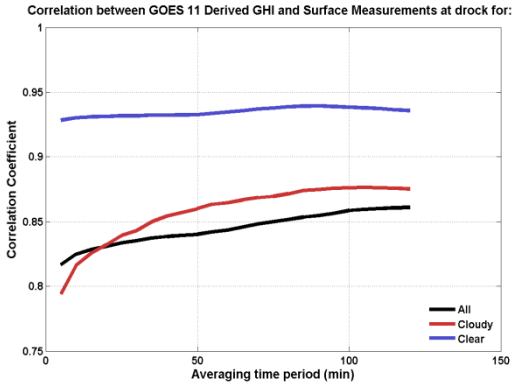

Figure A4. (C) MBE%, (D) RMSE%, and (E) correlation values under cloudy, clear, and all conditions for the Desert Rock, Nevada, site.

A

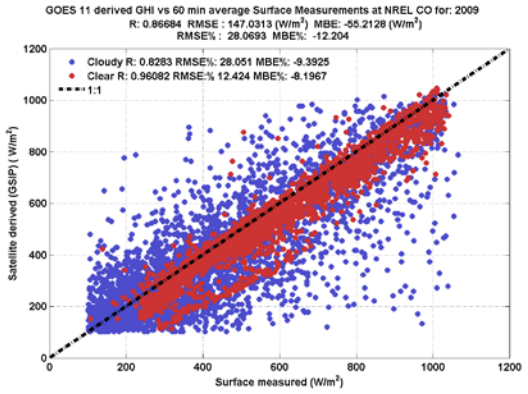

B

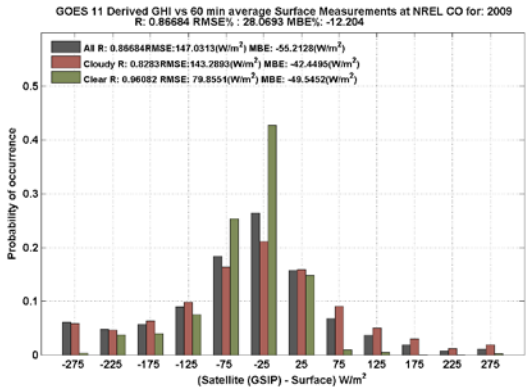

Figure A5. (A) Scatter plot and (B) probability distribution under clear and cloudy conditions for the NREL site in Golden, Colorado.

C

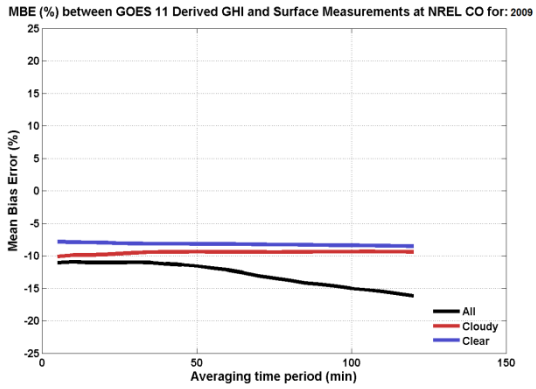

D

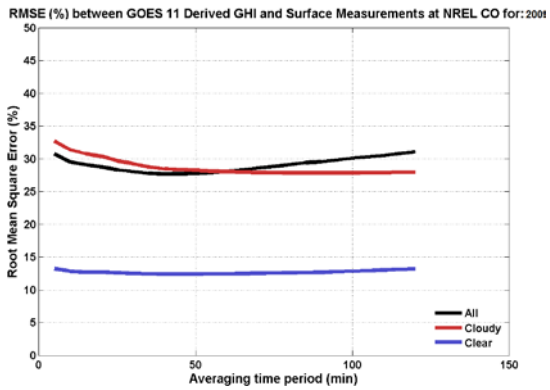

E

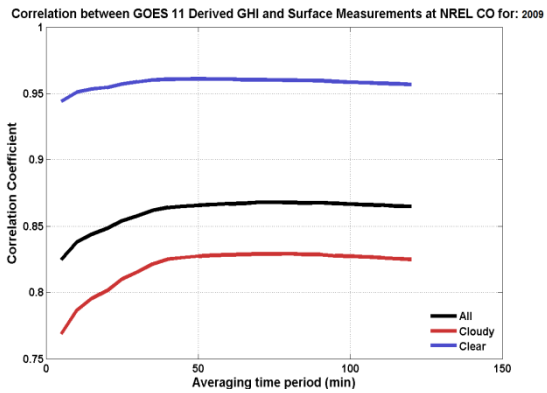

Figure A6. (C) MBE%, (D) RMSE%, and (E) correlation values under cloudy, clear, and all conditions for the NREL site in Golden, Colorado.

A

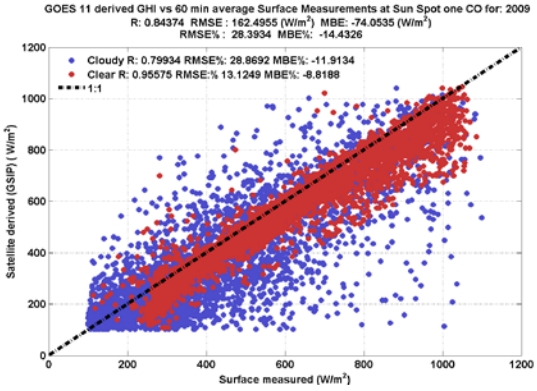

B

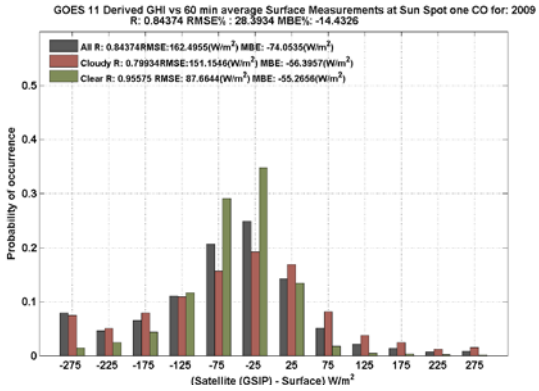

Figure A7. (A) Scatter plot and (B) probability distribution under clear and cloudy conditions for the SS1 site in San Luis Valley, Colorado.

C

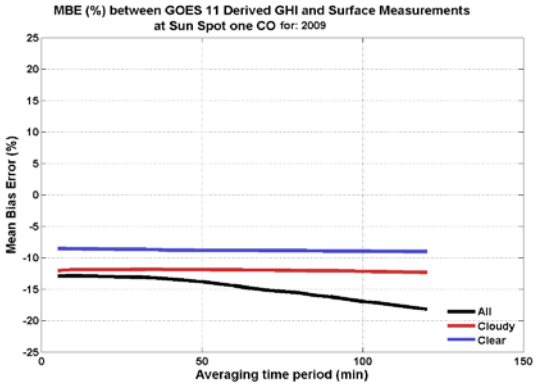

D

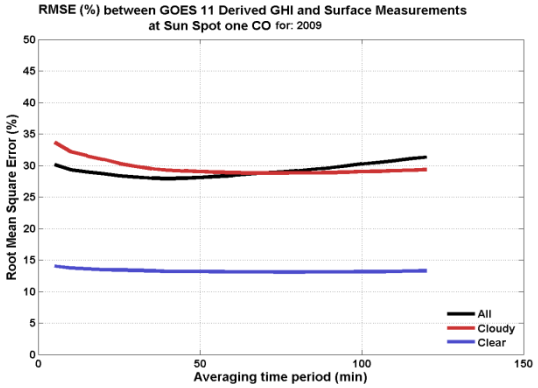

E

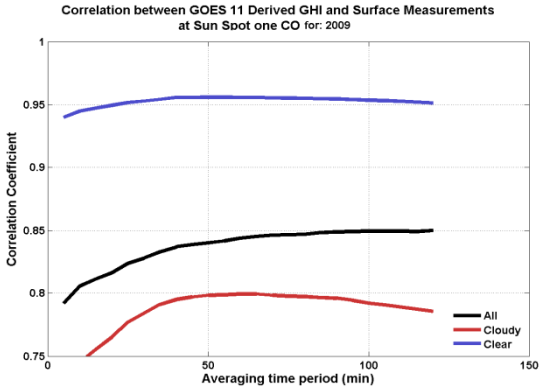

Figure A8. (C) MBE%, (D) RMSE%, and (E) correlation values under cloudy, clear, and all conditions for the SS1 site in San Luis Valley, Colorado.

A

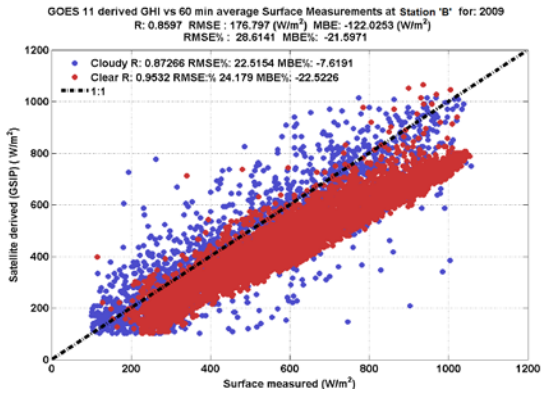

B

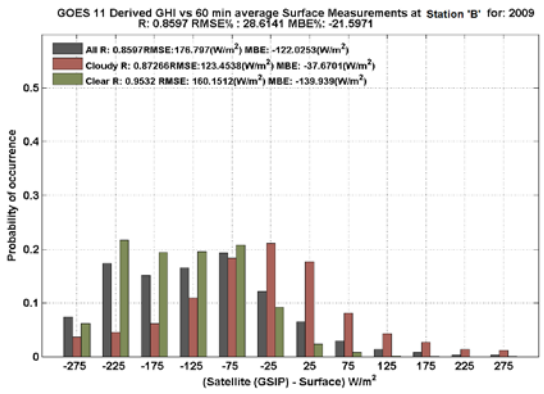

Figure A9. (A) Scatter plot and (B) probability distribution under clear and cloudy conditions for the Station B site.

C

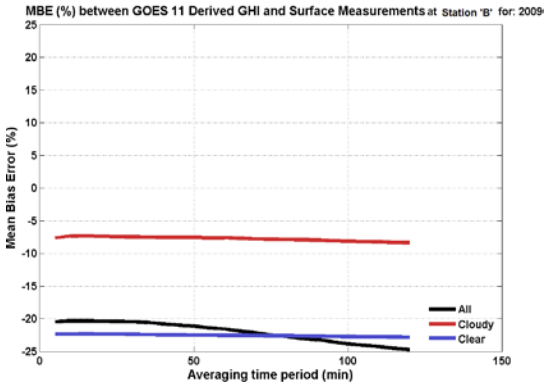

D

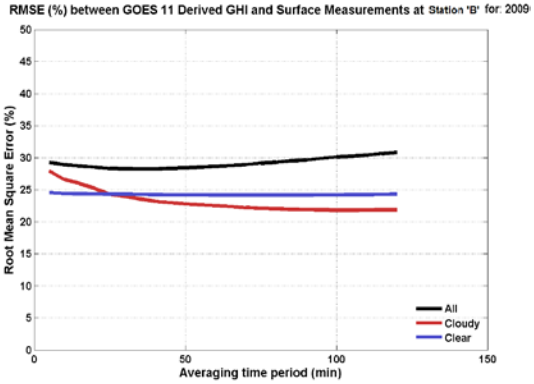

E

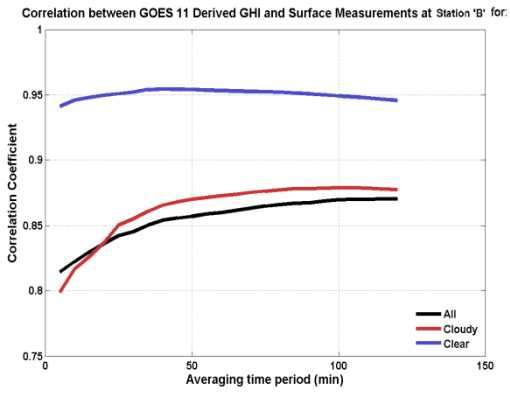

Figure A10. (C) MBE%, (D) RMSE%, and (E) correlation values under cloudy, clear, and all conditions for the Station B site.

A

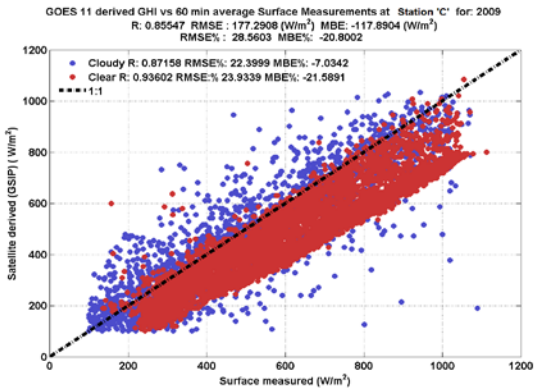

B

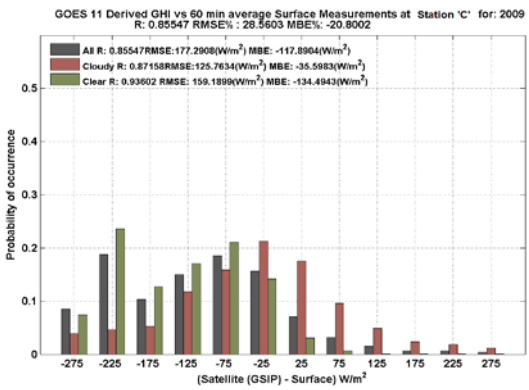

Figure A11. (A) Scatter plot and (B) probability distribution under clear and cloudy conditions for the Station C site.

C

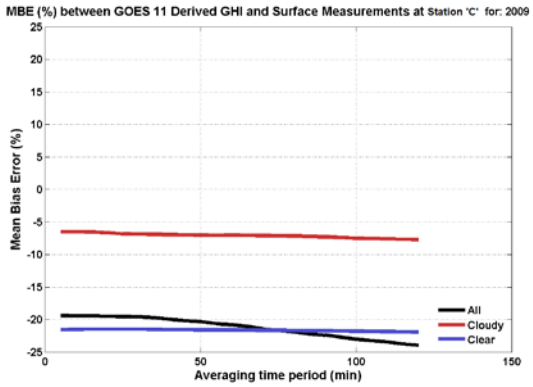

D

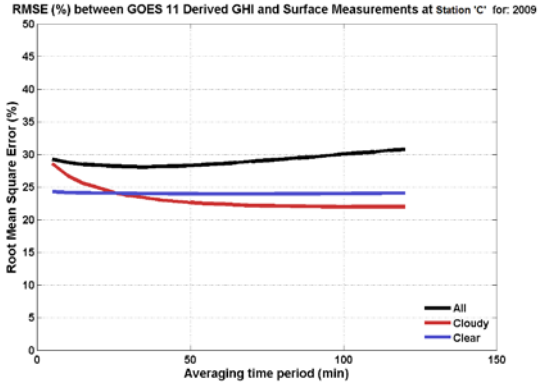

E

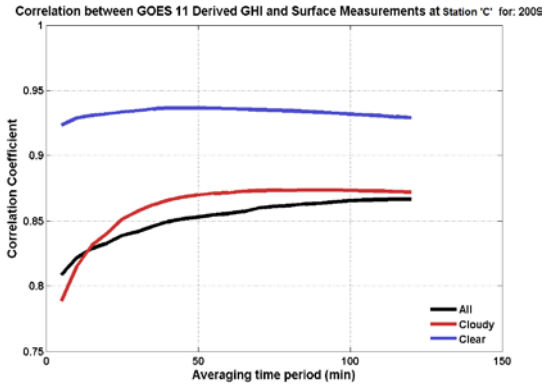

Figure A12. (C) MBE%, (D) RMSE%, and (E) correlation values under cloudy, clear, and all conditions for the Station C site.

A

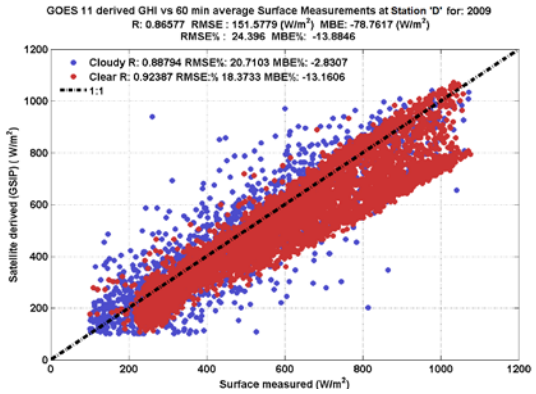

B

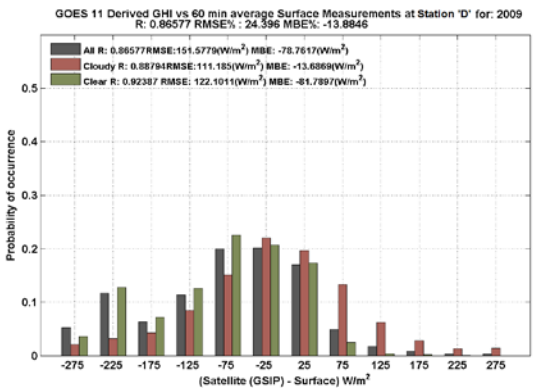

Figure A13. (A) Scatter plot and (B) probability distribution under clear and cloudy conditions for the Station D site.

C

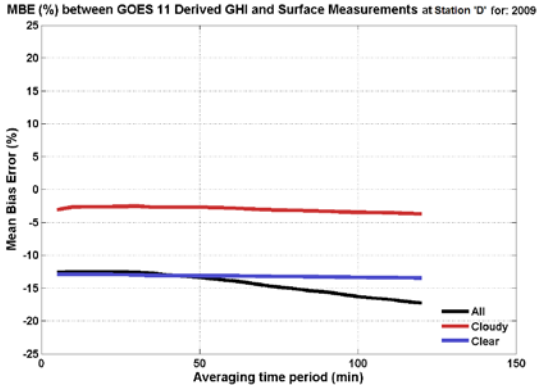

D

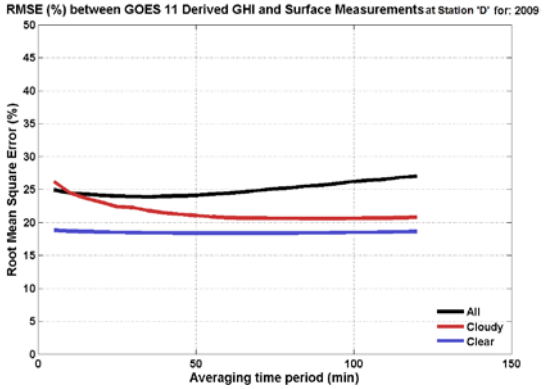

E

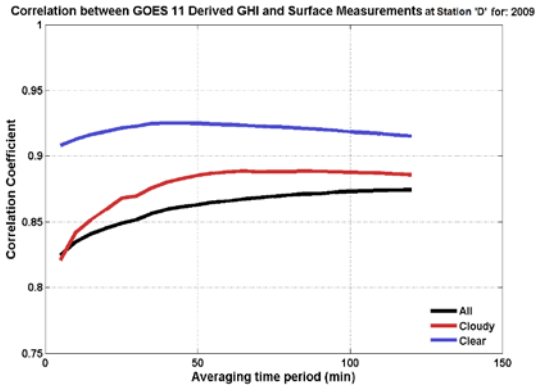

Figure A14. (C) MBE%, (D) RMSE%, and (E) correlation values under cloudy, clear, and all conditions for the Station D site.

A

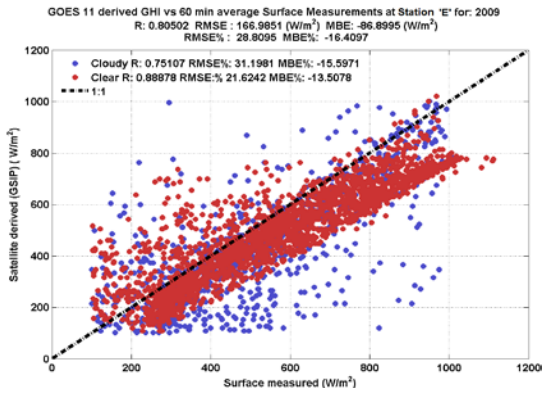

B

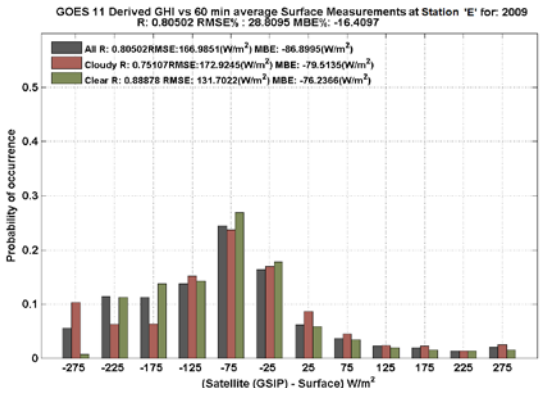

Figure A15. (A) Scatter plot and (B) probability distribution under clear and cloudy conditions for the Station E site.

C

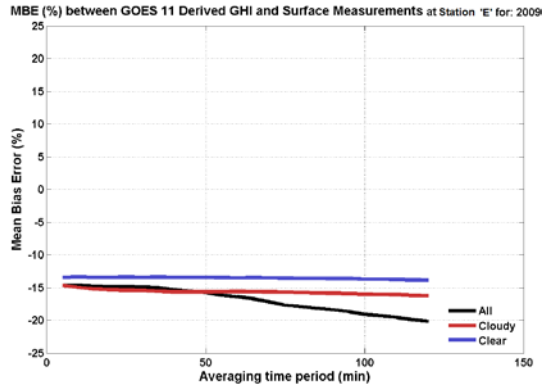

D

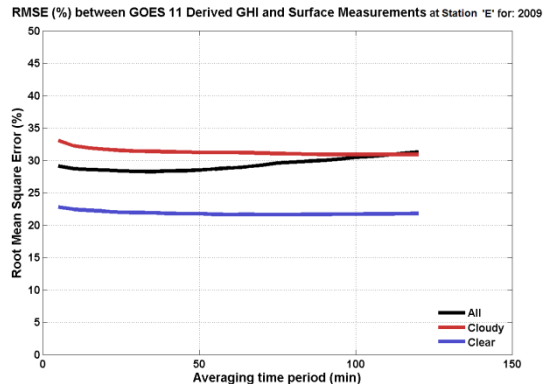

E

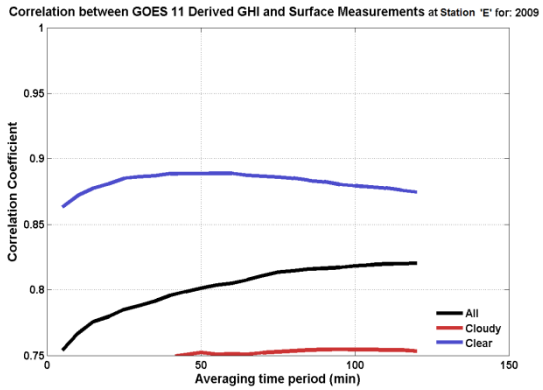

Figure A16. (C) MBE%, (D) RMSE%, and (E) correlation values under cloudy, clear, and all conditions for the Station E site.